



Searching for Extragalactic Exoplanetary Systems: The Curious Case of BD+20 2457

Hélio D. Perottoni¹ , João A. S. Amarante^{2,5} , Guilherme Limberg¹ , Helio J. Rocha-Pinto³ , Silvia Rossi¹ ,
Friedrich Anders⁴ , and Lais Borbolato¹

¹ Universidade de São Paulo, Instituto de Astronomia, Geofísica e Ciências Atmosféricas, Departamento de Astronomia, SP 05508-090, São Paulo, Brazil
hperottoni@gmail.com

² Jeremiah Horrocks Institute, University of Central Lancashire, Preston PR1 2HE, UK

³ Universidade Federal do Rio de Janeiro, Observatório do Valongo, Lad. Pedro Antônio 43, 20080-090, Rio de Janeiro, Brazil

⁴ Institut de Ciències del Cosmos, Universitat de Barcelona (IEEC-UB), Carrer Martí i Franquès 1, E-08028 Barcelona, Spain

Received 2021 March 16; revised 2021 April 12; accepted 2021 April 22; published 2021 May 18

Abstract

Planets and their host stars carry a long-term memory of their origin in their chemical compositions. Thus, identifying planets formed in different environments improves our understanding of planetary formation. Although restricted to detecting exoplanets within the solar vicinity, we might be able to detect planetary systems that formed in small external galaxies and later merged with the Milky Way. In fact, Gaia data have unequivocally shown that the Galaxy underwent several significant minor mergers during its first billion years of formation. The stellar debris of one of these mergers, Gaia-Enceladus (GE), is thought to have built up most of the stellar halo in the solar neighborhood. In this Letter, we investigate the origin of known planet-host stars combining data from the NASA Exoplanet Archive with Gaia EDR3 and large-scale spectroscopic surveys. We adopt a kinematic criterion and identify 42 stars associated with the Milky Way's thick disk and one halo star. The only halo star identified, BD +20 2457, known to harbor two exoplanets, moves on a retrograde and highly eccentric orbit. Its chemical abundance pattern situates the star at the border between the thick disk, the old halo, and accreted populations. Given its orbital parameters and chemical properties, we suggest that BD+20 2457 is likely formed in the protodisk of the Galaxy, but we do not exclude the possibility of the star belonging to the debris of GE. Finally, we estimate a minimum age and mass limit for the star, which has implications for its planetary system and will be tested with future Transiting Exoplanet Survey Satellite observations.

Unified Astronomy Thesaurus concepts: [Galaxy dynamics \(591\)](#); [Exoplanets \(498\)](#); [Milky Way stellar halo \(1060\)](#); [Galaxy kinematics \(602\)](#)

1. Introduction

The advent of surveys dedicated to searching for exoplanets covering large areas of the sky, e.g., Kepler mission (Borucki et al. 2010) and Transiting Exoplanet Survey Satellite (TESS) mission (Ricker et al. 2014), has increased the number of exoplanet candidates to 4325 around 3216 host stars.⁶ Consequently, the improvement of the statistical census of exoplanets (see Adibekyan 2019) contributes to a better understanding of, e.g., (i) the dependence of planet properties (e.g., giant planet occurrence, orbital features, and planetary composition) with its host star's chemical abundance (e.g., Gonzalez 1997; Fischer & Valenti 2005; Petigura et al. 2018; Teske et al. 2019), (ii) the planetary formation in different environments (Nayakshin 2017; Brassier & Mojzsis 2020), and (iii) the fraction of stars with exoplanets in our Galaxy (e.g., Raymond et al. 2007; Dressing & Charbonneau 2013, 2015; Hsu et al. 2019).

The universality of the aforementioned features are yet to be tested; it will be achieved only with the study of exoplanets in external galaxies. Up to now, only a few planetary-mass objects have been found in extragalactic systems through microlensing events (see Dai & Guerras 2018; Bhatiani et al. 2019; Di Stefano et al. 2020). This is mainly due to the current impossibility to use the traditional detection methods, radial velocity and transit, in resolved stellar sources at large distances. In principle, it could be done in the future for, e.g.,

M31 (Ingrosso et al. 2009), Large Magellanic Cloud (Lund et al. 2015), and Small Magellanic Cloud (Mróz & Poleski 2018). Nonetheless, we do not need to search for exoplanets in nearby galaxies to study extragalactic planetary systems: the Milky Way (MW) may already host exoplanets from accreted dwarf galaxies.

The Galaxy experienced a significant accretion event ~ 10 Gyr ago (at redshift $z \sim 2$) with a dwarf galaxy named Gaia-Enceladus (GE; Belokurov et al. 2018; Helmi et al. 2018). The stars accreted from this event constitute most of the nearby/inner halo, i.e., within at least 3 kpc from the Sun (e.g., Haywood et al. 2018; Di Matteo et al. 2019). Carrillo et al. (2020) used a sample of TESS candidates cross-matched with Gaia and showed that $\sim 1\%$ TESS target stars inhabit the Galactic stellar halo (hereafter "halo"; their Figure 4 clearly shows the kinematic signature of GE). This opens the possibility to investigate extragalactic exoplanets in stars that were accreted during this event.

With this motivation, we investigated the dynamical properties of known exoplanet-host stars looking for systems with halo-like orbits. With data from Gaia Early Data Release 3 (GEDR3) and large-scale ground-based spectroscopic surveys, we found a strong candidate that we further investigate according to its abundances. The Letter is organized as follows. Section 2 describes the data used in our analysis; Section 3 shows the kinematics, orbital parameters, and abundances of the exoplanet-host stars that likely belong to the MW's thick disk and halo; Section 4 describes the BD+20 2457 system and discusses its possible chemodynamical origin and implications

⁵ Visiting Fellow.

⁶ According to NASA Exoplanet Archive in 2020 December.

to its planetary system; finally, in Section 6, we provide our conclusions and final remarks. We also include three appendices. Appendix A describes the quality control applied to the data, Appendix B describes the traditional kinematical selection criteria according to Bensby et al. (2003), and Appendix C presents a table of exoplanets classified as thick disk or halo and some of their features.

2. Data

This Letter is based on a combination of data from the Exoplanet Archive with APOGEE DR16, GEDR3, GALAH DR3, and LAMOST DR5 (Cui et al. 2012; Gaia Collaboration et al. 2021; Akeson et al. 2013; Buder et al. 2021; Ahumada et al. 2020; see Appendix A for details about the sample selection criteria). We build four samples of planet-host stars containing the five astrometric parameters and their uncertainties from the GEDR3 catalog and radial velocities and errors from either the aforementioned spectroscopic surveys or Gaia itself. Our combined sample contains 1559 planet-host stars and the individual samples from APOGEE, Gaia, GALAH, and LAMOST have 682, 919, 116, and 453 stars, respectively. In addition to that, we selected a cleaned sample of stars from APOGEE DR16 (see Appendix A) to illustrate some of the features that will be presented. We refer to it as the APOGEE sample throughout the Letter.

We calculated the orbits of the stars with the publicly available Python library AGAMA (Vasiliev 2019) for ~ 5 Gyr forward. The Galactic potential model employed is described in McMillan (2017). We adopt the values from Bovy (2020) for the solar Galactocentric distance $R_{\odot} = 8.22$, the local circular velocity $v_c = 243.0 \text{ km s}^{-1}$, and the solar motion with respect to the local standard of rest $(U_{\odot}, V_{\odot}, W_{\odot}) = (11.10, 7.20, 7.25) \text{ km s}^{-1}$. We tested with other sets of fundamental Galactic parameters, e.g., those recommended by McMillan (2017), and concluded that our main results do not depend on these choices.

For each star, we performed 1000 Monte Carlo realizations of the orbit according to Gaussian distributions of its uncertainties in the phase-space coordinates. The medians of each kinematic/dynamical quantity considered are taken as our nominal values. The adopted uncertainties are the 16th and 84th percentiles of the resulting distributions. In this work, our analyses are based on the complete velocity vector $(v_R, v_{\phi}, \text{ and } v_z)$ of each star in the cylindrical coordinate system (radial, azimuthal, and vertical directions, respectively), the maximum distance from the Galactic plane achieved during a star’s orbit (Z_{max}), the perigalactic (r_{min}) and apogalactic (r_{max}) distances, eccentricity ($e = (r_{\text{max}} - r_{\text{min}})/(r_{\text{max}} + r_{\text{min}})$), total orbital energy (E), and vertical component of the angular momentum $L_z = R_{\text{Gal}} \times v_{\phi}$, where R_{Gal} is the plane-projected distance of a given star from the Galactic center.

3. Analysis

The Toomre diagram is generally used to kinematically classify halo and/or thick-disk stars (e.g., Bensby et al. 2003). Given assumptions on the properties of the stellar populations (namely, their relative fractions and velocity distributions), we can predict which regions of the v_{ϕ} versus $\sqrt{v_R^2 + v_z^2}$ plane will be dominated by a given population. We used the Galaxia model (Sharma et al. 2011)—with an updated description of the thick disk and stellar halo velocity distributions and their local fractions (as described in Amarante et al. 2020b)—to define the

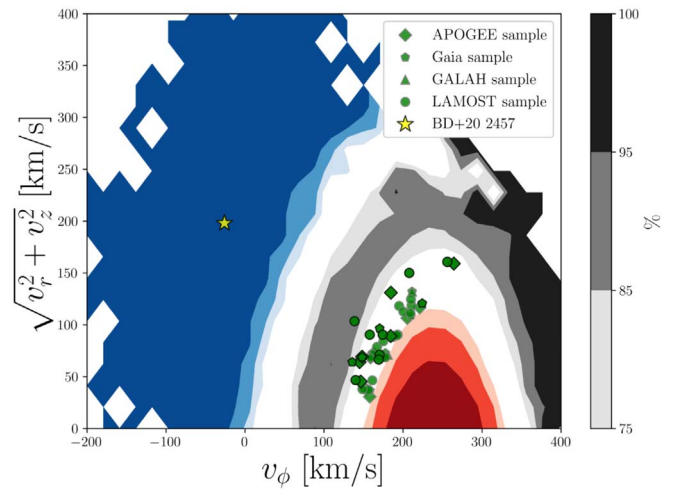


Figure 1. Toomre diagram of the halo/thick-disk host stars. The thin disk, thick disk, and halo are represented by the red, gray, and blue colors, respectively. The darkness in shading corresponds to the fraction of a given population at that location of the diagram (75%, 85%, or 95%). The host stars classified as thick-disk and halo stars are shown in green and yellow, respectively. The symbols with a black contour are the host stars classified as thick-disk stars ($TD/D > 10$) according to the kinematic criteria of Bensby et al. (2003).

regions of the diagram where each population dominates. This is illustrated in Figure 1. The thin disk, thick disk, and halo are represented by the red, gray, and blue shaded areas, respectively. The darkness in the shading corresponds to regions where a given population has a fraction greater than 75%, 85%, or 95% overall. According to our criteria, thick-disk stars are all the objects that lie outside of the thin-disk predominant region. We used this diagram to initially select stars in our sample that are likely to belong to the halo.

Overplotted in Figure 1, we show only the stars in our sample that were not classified as thin disk. According to our criteria, we identified 42 planet-host stars as thick-disk candidate stars⁷ (see Table in Appendix C). We also applied a formalism similar to Bensby et al. (2003; see Appendix B) to classify our thick-disk candidates according to a second kinematic criterion. The stars classified as thick disk according to this method, those having thick-disk-to-thin-disk (TD/D) membership ratios higher than 10, are shown with a black contour in Figure 1. Our final list contains 18 highly probable thick disk and 1 halo candidates. Thick-disk planet-host stars were previously confirmed to exist (e.g., Gan et al. 2020 for a recent discussion) and are important constraints to the planetary formation theory, but in this Letter we focus on the host star having halo-like characteristics.

The only star we found in the halo-dominated region results in a fraction of 0.06% of halo planetary host stars in our sample. While this relatively fraction seems low, we note that TESS is expected observe 0.16% of halo stars (Carrillo et al. 2020). If halo stars have the same probability of disk stars to host a planet, $\sim 30\%$ (e.g., Zhu & Dong 2021), finding only one exoplanetary system in the halo is within the expectations given our sample size.

Figure 2 shows the orbital properties of the host stars. We also included as gray dots the APOGEE sample, within 2 kpc from the Sun, for comparison. The left panel shows the E - L_z plane, where

⁷ Stars classified as thick disk in more than one sample are counted as one object.

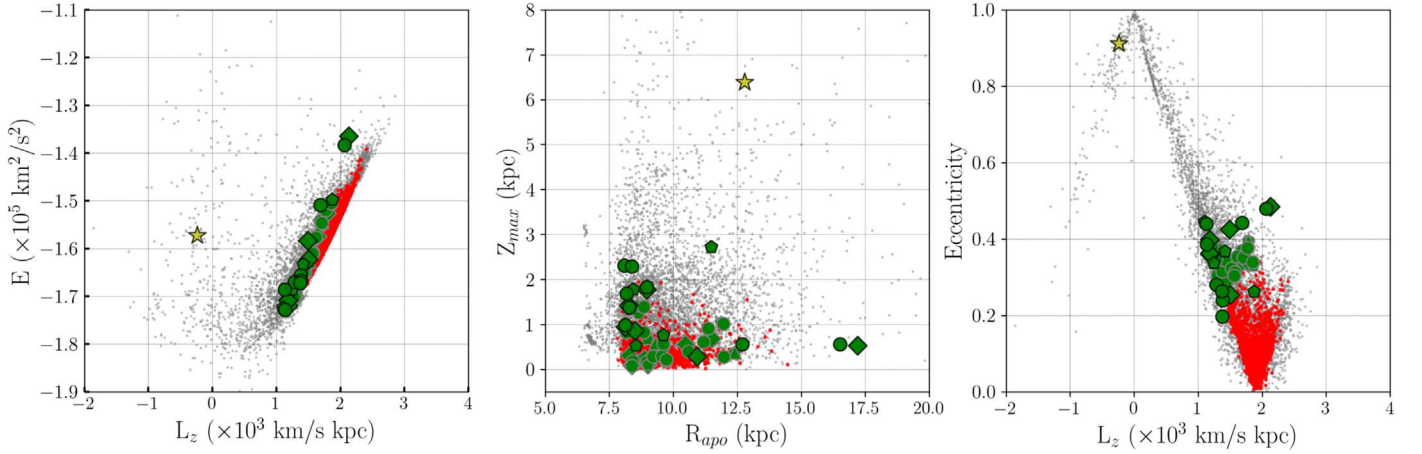


Figure 2. The orbital parameters of host stars in the E - L_z (left), Z_{\max} - r_{\max} (middle), and eccentricity- L_z (right) planes. The halo host star BD+20 2457 is represented as a yellow star symbol. The host stars classified as belonging to the thick and thin disks are shown in green and red symbols, respectively. The gray dots are stars from the APOGEE sample, within a heliocentric radius of 2 kpc, which we used to illustrate the local stellar distribution. The green symbols are defined as in Figure 1.

the thick-disk host stars (green circles) have smaller L_z compared to the thin-disk ones (red circles), at the same E . The middle panel shows that, as expected, thick-disk host stars have larger vertical excursions from the plane ($\langle Z_{\max} \rangle = 1.28$ kpc) compared to thin-disk ones ($\langle Z_{\max} \rangle = 0.32$ kpc). Finally, the eccentricity- L_z plane (right panel) shows that the majority of thick-disk host stars have lower average vertical component of the angular momentum and higher eccentricity ($\langle L_z \rangle = 1.43 \times 10^3$ kpc km s $^{-1}$; $\langle e \rangle = 0.35$) compared to the thin disk ($\langle L_z \rangle = 1.87 \times 10^3$ kpc km s $^{-1}$; $\langle e \rangle = 0.11$). All the aforementioned properties are in line with expectations given the kinematic characteristics of both populations and in agreement with previous studies that investigated the chemically defined thin- and thick-disk properties (see Li et al. 2018).

Interestingly, the host star BD+20 2457 has kinematics and dynamics typical of a halo star (yellow star symbol in Figures 1 and 2). It is on a retrograde orbit, $L_z = -235$ kpc km s $^{-1}$, with high eccentricity, $e = 0.91$, and it reaches $Z_{\max} = 6.39$ kpc from the Galactic plane. Besides, BD+20 2457 is located in a region of E - L_z space dominated by accreted stars (see Helmi 2020 for a review). The recently discovered GE is the most prominent kinematic stellar structure that overlaps with this star in all the orbital spaces (see Limberg et al. 2021 and references therein), including a stricter criterion: Feuillet et al. (2020) recommend a cut on the radial action of stars, $^8 \sqrt{J_R} > 30$ kpc km s $^{-1}$, to select a “pure” GE sample. We find a radial action of $\sqrt{J_R} = (29.9 \pm 0.2)$ kpc km s $^{-1}$, which means that BD+20 2457 is compatible with such a conservative criterion at the 1σ level.

4. BD+20 2457: An Intriguing Star

Having found the most likely host-star candidate to be originated from an accreted galaxy, BD+20 2457, we now proceed to explore its elemental abundances and discuss its origin and implications toward this particular star-planet system.

4.1. Chemistry

We explore the elemental abundances of BD+20 2457 to investigate whether its chemical profile is also similar to that

from GE. We adopted $[\text{Fe}/\text{H}]$, $[\text{Mg}/\text{Fe}]$, $[\text{Mg}/\text{Mn}]$, and $[\text{Al}/\text{Fe}]$ from the high-resolution ($R \geq 67,000$) spectroscopic study of Maldonado et al. (2013). Figure 3 shows the abundance planes that are commonly used to depict accreted stars from in situ populations. The dashed lines in the top panel segregate stars into thin disk, thick disk, and accreted halo following Mackereth et al. (2019a). The red contours in all the panels define the chemistry associated with accreted stars according to Das et al. (2020). For comparison, we also show the APOGEE sample as the 2D histogram. Despite having halo-like kinematics and dynamics, BD+20 2457 has a chemical pattern consistent with the regions dominated by the chemical thick disk.

However, we cannot immediately rule out the possibility that BD+20 2457 was born in the GE’s progenitor system since this substructure is expected to have a large spread in abundances (Matsuno et al. 2019), commensurate with a massive progenitor. In fact, in Figure 3, we also show that a small number of GE stars (gray dots) that were selected from the APOGEE sample ($[\text{Fe}/\text{H}] < -0.5$), following Feuillet et al.’s (2020) conservative selection criteria, have chemical properties similar to BD+20 2457 and thick-disk stars.

With the ambiguity brought from the chemodynamical analysis of BD+20 2457 star, we proceed with a more detailed investigation on the origins of this star.

4.2. Accreted or Heated?

The accretion event of the massive dwarf galaxy GE (Belokurov et al. 2018; Helmi et al. 2018) occurred ~ 10 Gyr ago (Gallart et al. 2019; Montalbán et al. 2020) and is thought to be responsible for the formation of the thick disk either by dynamical heating (Bignone et al. 2019; Di Matteo et al. 2019; Gallart et al. 2019) or by an induced star formation burst (Bignone et al. 2019; Grand et al. 2020).

The stellar debris from this merger dominate the inner halo (Haywood et al. 2018; Di Matteo et al. 2019; Naidu et al. 2020), although the latter also has a more metal-rich counterpart proposed to be formed in situ (Bonaca et al. 2017; Gallart et al. 2019) and heated to halo-like orbits (Di Matteo et al. 2019; Gallart et al. 2019; Amarante et al. 2020b; Grand et al. 2020). Belokurov et al. (2020) suggested that the metal-rich portion of the inner halo is a distinct component of the Galaxy

⁸ The radial action J_R represents the radial excursion of a given star in an axisymmetric potential (Binney & Tremaine 2008).

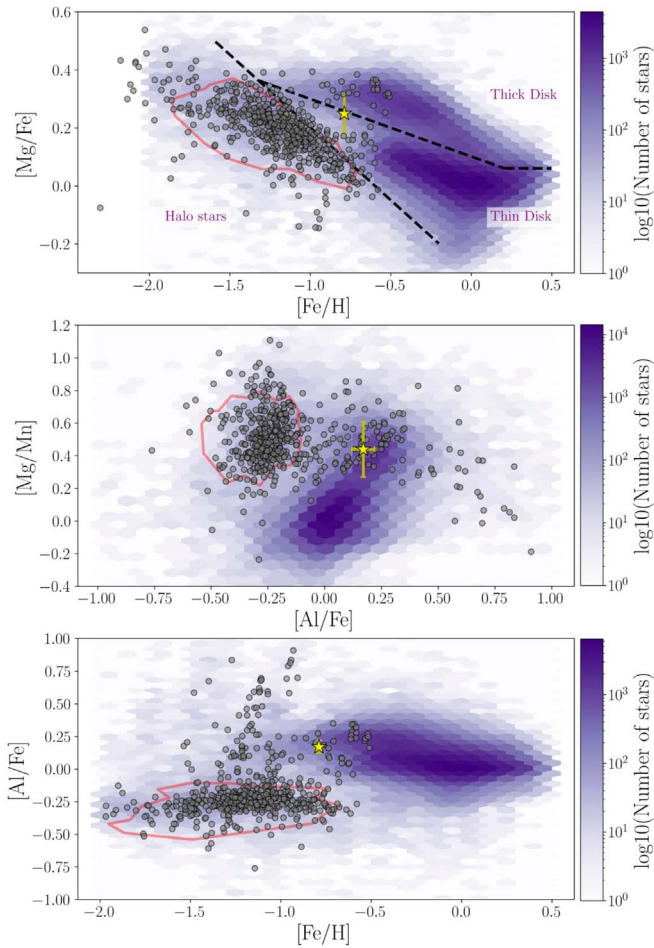


Figure 3. The chemical abundances of the host star BD+20 2457 (yellow star) in $[\text{Fe}/\text{H}]$ and $[\text{Mg}/\text{Fe}]$ (top), $[\text{Mg}/\text{Mn}]$ and $[\text{Al}/\text{Fe}]$ (middle), and $[\text{Al}/\text{Fe}]$ and $[\text{Fe}/\text{H}]$ (bottom). The gray dots are GE candidate stars selected according to Feuillet et al. (2020) from the APOGEE sample cut in $[\text{Fe}/\text{H}] < -0.5$. The black dashed line is used to separate three main stellar groups according to Mackereth et al. (2019a). The red contour indicates the “blob” of accreted stars (Das et al. 2020). The 2D histogram color coded background shows the distribution of the APOGEE sample stars.

and called it “Splash.” According to this hypothesis, the Splash was part of the protodisk of the Galaxy that was dynamically heated to halo-like orbits.

In this context, the metal-rich component of the inner halo has v_ϕ , metallicity distributions, and several orbital parameters (Belokurov et al. 2020, see their Figure 1) that are in agreement with the values obtained for BD+20 2457. The main difference is that the nearby Splash stars typically do not reach values of $Z_{\text{max}} > 4$ kpc. Thus, the scenario of a merger event that dynamically heated the protodisk appears to explain the puzzling thick-disk-like chemical composition and the halo-like orbit of BD+20 2457. Alternatively, Amarante et al. (2020a) pointed out that a Splash-like population, i.e., a heated thick disk, could already be present in the young Galaxy during the GE merger event due to an early clumpy formation. Although it adds an extra puzzle regarding the BD+20 2457 origin, the clumpy formation would have occurred during the first gigayears of the Galaxy (Clarke et al. 2019) and thus is also able to constrain BD+20 2457’s age as will be discussed in Section 5.

In Section 4.1, we showed that BD+20 2457 has abundances typical of the thick disk, but also that some dynamically

selected GE candidates overlap with the thick disk in chemical parameter space. This is also seen in Matsuno et al. (2021, see their Figure 4) for the $[\text{Mg}/\text{Fe}]$ ratio from a GE sample selected from GALAH DR3. In an attempt to quantify the rarity of stars with the same chemical and orbital properties of BD+20 2457, we search in the APOGEE sample for stars that have $[\text{Fe}/\text{H}]$, $[\text{Mg}/\text{Fe}]$, $[\text{Mg}/\text{Mn}]$, and $[\text{Al}/\text{Fe}]$ within an interval of ± 0.1 dex from the abundances of BD+20 2457. Although not perfect, such monoabundance selection enables the study of coeval populations properties (e.g., Bovy et al. 2012; Beraldo e Silva et al. 2020). We found that 1270 stars satisfy these criteria but only 3 stars (0.2%) were dynamically selected as GE candidates (Feuillet et al. 2020). This may indicate that protodisk stars when heated typically do not have GE-like orbits or that the fraction of GE contamination in the chemical abundance space is very small. In either case, further investigations are necessary to estimate the fraction of stars with these characteristics that could be related to either GE or Splash.

We also estimated how likely is BD+20 2457 to belong either to the thick disk or GE based on the ($[\text{Fe}/\text{H}]$, $[\text{Mg}/\text{Fe}]$, $[\text{Al}/\text{Fe}]$, $[\text{Mg}/\text{Mn}]$) chemical space. We calculated a multivariate KDE with the R-package *ks* (Chacón & Duong 2018), and derived a chemical thick-disk-to-GE likelihood ratio. This is a similar approach used by Bensby et al. (2003) in the kinematic space. In our analysis, the thick-disk sample was selected according to Mackereth et al. (2019b), shown in Figure 3, and the GE candidate stars were selected according to Feuillet et al. (2020). We found that BD+20 2457 has a chemical thick-disk-to-GE likelihood ratio $\gg 1000$, which reinforces our preliminary analysis that it is chemically more akin to the thick disk.

Finally, we can exclude that any sort of bar interaction could be the cause of the retrograde motion and eccentric orbit observed for this star. Fiteni et al. (2021) showed that bars can only drive retrograde motion in the vicinity of the bar (see their Figure 5), i.e., within ~ 5 kpc from the Galactic center of the Milky Way (Bland-Hawthorn & Gerhard 2016).

The aforementioned facts indicate that BD+20 2457 is likely from the protodisk, but we do not completely rule out the possibility of it being an accreted star, due to the lack of studies of the chemical evolution of GE. Either way, this detailed chemodynamical analysis of BD+20 2457 origin has important implications to its mass and age as we will discuss in the following section.

5. Mass and Age of BD+20 2457

The BD+20 2457 system was discovered by Niedzielski et al. (2009). According to the authors, the host star is a K2 II giant with $2.8 M_\odot$, and the exoplanets BD+20 2457 b and BD+20 2457 c have $12.5 M_J$ and $21.4 M_J$, respectively. The host star has an apparent G -band magnitude $G = 9.234 \pm 0.003$ mag, $\varpi = 0.6787 \pm 0.02$ mas, $(\mu_\alpha^*, \mu_\delta) = (-35.952 \pm 0.019; -29.96 \pm 0.018)$ mas yr $^{-1}$, and $\text{RV} = 145.77 \pm 0.19$ km s $^{-1}$ (Gaia Collaboration et al. 2021). Its atmospheric parameters are $T_{\text{eff}} = 4258 \pm 13$ K, $\log g = 1.64 \pm 0.07$ (cgs), and $[\text{Fe}/\text{H}] = -0.79 \pm 0.02$ dex (Maldonado et al. 2013). However, there is no consensus on the host star’s mass in the literature; it is reported to vary from 0.8 to $10.83 M_\odot$ (Zieliński et al. 2012; Stassun et al. 2017). These differences in the stellar mass have important implications to the planetary masses reported originally by Niedzielski et al. (2009).

We used *StarHorse* (Queiroz et al. 2018) to estimate an isochrone mass and age for this star using the spectroscopic data of Maldonado et al. (2013), the GEDR3 parallax, and multiwavelength photometric measurements from Gaia, 2MASS (Skrutskie et al. 2006), and AllWISE (Wright et al. 2010) as input. When correcting for the parallax zero-point offset for this star (see Appendix A), we find that ages anywhere between 2 and 11 Gyr (masses between 0.9 and 1.5 M_{\odot}) are possible. The exact choices of the priors, the calibrations of parallax, surface gravity, and effective temperature, and their associated uncertainties, as well as considerable stellar model uncertainties in the upper red giant branch make it almost impossible to establish a reliable and precise age for BD+20 2457 without asteroseismic measurements. Nonetheless, we are still able to constrain its age and mass based on its chemistry and dynamics.

First, we tested the hypothesis of BD+20 2457 as an old star through an estimation of the kinematic age of a population likely coeval with it. We use the same monoabundance population selected from the APOGEE sample (see Section 4.2) and confirm that their velocity dispersions are commensurate with an old population, i.e., age >8 Gyr, according to the age–velocity dispersion relations of the monoabundance populations in Mackereth et al. (2019b). This confirms that stars with chemical abundances such as BD+20 2457 are very unlikely to be young, i.e., age <2 Gyr.

Second, as discussed in Section 4.2, stars with halo-like kinematics and thick-disk abundances are most likely part of the heated protodisk. Furthermore, according to the assumption that the Galaxy’s last significant merger was GE (Grand et al. 2020), the protodisk stars were heated during this event or before, e.g., during a clumpy phase of disk. Therefore, we can use the epoch of the GE event to constrain BD+20 2457’s age, and thus its mass. Several authors, using observations and/or simulations, converge on an estimated epoch for merger event between 9 and 11 Gyr ago (e.g., Belokurov et al. 2018; Helmi et al. 2018; Bonaca et al. 2020). As the dynamical effects of the merger on the protodisk can last for ~ 1 Gyr (Bignone et al. 2019; Bonaca et al. 2020; Grand et al. 2020), we suggest that BD+20 2457 must be older than 8 Gyr, commensurate with direct age estimation of GE stars from (Gallart et al. 2019; Montalbán et al. 2020).

Finally, based on the chemodynamical arguments and with the host star’s metallicity and $[\alpha/\text{Fe}]$ (Maldonado et al. 2013), we obtained a synthetic isochrone from the Dartmouth Stellar Evolution Database (Dotter et al. 2008) and constrained the host star’s mass to an upper limit of 1.00 M_{\odot} .⁹ This results in planetary masses of $m \sin i \sim 13$ and 7 M_J for BD+20 2457 b and BD+20 2457 c, respectively. These values are $\sim 50\%$ smaller compared to Niedzielski et al. (2009).

6. Conclusions and Final Remarks

In this Letter, we investigated the origin, in situ or accreted, of known planet-host stars. We combined the NASA Exoplanet Archive with GEDR3 and large ground-based spectroscopic surveys (namely, APOGEE DR16, GALAH DR3, and LAMOST DR5) and calculated the host stars’ kinematic and dynamical parameters. Among the large sample of the thin-disk stars (97.2% of the sample), we were able to identify 42 (2.7%

of the sample) thick-disk planet-host stars based on our kinematic criteria (see Section 3) and, most interestingly, a star with halo-like kinematics and dynamics: BD+20 2457.

Although the orbit of BD+20 2457 is very similar to what is commonly associated with GE stars, its chemical abundances are typical to what is associated with the thick-disk of the MW (see Section 4.2). Based on this finding, we suggest that BD+20 2457 is most likely a star born in the MW’s protodisk. But we cannot rule out the possibility of this star being formed in the GE as its chemical evolution is yet to be well understood.

The association of BD+20 2457 with the Galactic protodisk, or even with GE, has an important implication to its planetary system: it can constrain the host star’s age and, therefore, its mass, which are not well defined in the literature (see Section 5). Moreover, the current mass estimation indicates that the BD+20 2457 system is dynamically unstable on a short timescale (Horner et al. 2014). Then, we took into account the epoch of the GE merging event and were able to constrain the minimum age and the mass’ upper limit of BD+20 2457: 8 Gyr and 1.00 M_{\odot} , respectively. This decreases the estimated masses of its planets BD+20 2457 b and BD+20 2457 c in about 50%.

Our prediction can be tested once asteroseismological data for BD+20 2457 become available, enabling more precise estimates for its mass and age. We note that TESS is due to observe this star in 2021 November.¹⁰

While this Letter was being written, Chen et al. (2021) presented a study that also classified planet-host stars into different Galactic components according to their kinematics. Their selection criteria removed BD+20 2457 due to its relative parallax error being greater than 10% in Gaia DR2. In GEDR3, whose data was employed in this work, the relative parallax error is $<3\%$. They also classified Kapteyn’s star (HD 33793) as a halo member, but this object was outside the cross-match range between NASA Exoplanet Archive and GEDR3 (see Appendix A). Despite that, we investigated Kapteyn’s star and it also has a heated disk-like orbit—with a much lower vertical excursion from the Galactic plane ($Z_{\text{max}} = 0.82$ kpc) compared to BD+20 2457—in conformity with its chemical properties (Woolf & Wallerstein 2004), more likely to belong to the heated disk.

This Letter provides a clear demonstration that, thanks to the Gaia mission and large-scale spectroscopic surveys, extragalactic exoplanets can already be found inhabiting the Galactic stellar halo. Despite the origin of BD+20 2457 remaining unclear, our analysis inaugurates the exciting possibility of searching for exoplanet-host stars with chemodynamical signatures similar to that of accreted populations. Stars in the nearby halo have the enormous advantage of being much closer, hence significantly brighter, than any surviving satellite galaxy, thus allowing for immediate asteroseismic and/or high-resolution spectroscopic follow-up. With this approach, studies of the phenomena of planet formation in different environments will certainly be facilitated. We note that there are many millions of TESS targets still to be observed, thousands of which overlap with the kinematic footprint of GE (Carrillo et al. 2020). Our group is currently working on the construction of a catalog of likely accreted TESS targets to be made publicly available to the astronomical community. In this scenario, it is reasonable to conjecture that the first extragalactic exoplanet, even if BD+20 2457 is not one

⁹ The isochrone does not take into account the mass lost by the star over its lifetime.

¹⁰ According to <https://heasarc.gsfc.nasa.gov/cgi-bin/tess/webtess/wtv.py>.

such system, will be discovered in the Milky Way itself in the upcoming years.

We thank the anonymous referee for useful comments that helped to improve this work. We also thank Thaise Rodrigues for helpful discussions about Bayesian methods to estimate stellar ages; Rodrigo Bouffleur for discussions about exoplanet masses; and Daniel Holdsworth for discussions about TESS mission. H.D.P. thanks FAPESP Proc. 2018/21250-9, G.L. acknowledges CAPES (PROEX; Proc. 88887.481172/2020-00). S.R. would like to acknowledge support from FAPESP (Proc. 2015/50374-0 and 2014/18100-4), CAPES, and CNPq. F.A. acknowledges financial support from MICINN (Spain) through the Juan de la Cierva-Incorporación program under contract IJC2019-04862-I. L.B. acknowledges CNPq/PIBIC (Proc.136092/2020-9).

This research has made use of the NASA Exoplanet Archive, which is operated by the California Institute of Technology, under contract with the National Aeronautics and Space Administration under the Exoplanet Exploration Program.

This research has been conducted despite the ongoing dismantling of the Brazilian scientific system.

Appendix A Quality Control Cuts

We impose astrometric and spectroscopic quality cuts to obtain more precise and reliable orbital parameters. Below, we describe the adopted quality control cuts for each catalog data.

1. We selected only Gaia EDR3 stars with high-quality parallaxes ($\varpi/\sigma_\varpi > 5$) and with good astrometric solutions ($\text{RUWE} < 1.4$; Lindegren et al. 2021a). We computed the distances as $d = 1/\varpi$ considering an offset of -0.017 mas (Lindegren et al. 2021b).
2. We discarded APOGEE DR16 sources with bad spectroscopic flags $\text{ASPCAPFLAG} \neq 0$ and $\text{STARFLAGS} = \text{SUSPECT_RV_COMBINATION}$ to select stars with good estimates of radial velocities.
3. We selected only GALAH DR3 stars with the flag parameter $\text{flag_sp} = 0$ to ensure the quality of spectra and data.
4. We obtained the LAMOST data from the added-value catalog of Xiang et al. (2019). We selected stars with r -band signal-to-noise ratio (S/N) larger than 5, g -band S/N larger than 10, i -band S/N larger than >10 , and quality flag $\text{qflag_chi2} = \text{good}$ and $\text{qflag_singlestar} = \text{YES}$.
5. The APOGEE sample has the same flags of item 2 and we applied additional cuts ($4000 < T_{\text{eff}} < 6000$, $1 < \log g < 3$, and S/N larger than 70) in order to select only giant stars with high-quality elemental abundances.

Table 1
Parameters for the Velocity Ellipsoid for Each Galactic Component

	X	σ_{v_R}	σ_{v_ϕ}	σ_{v_z}	V_{asym}
Thin disk (D)	0.9301	30	20	18	-28
Thick disk (TD)	0.0652	61	45	44	-63
Halo (H)	0.0047	160	119	110	-228

In order to build the samples, we performed a 3 arcsec radius cross-match between GEDR3 and the catalogs using TOPCAT (Taylor 2005).

Appendix B Kinematical Selection Criteria

We have adapted the formalism by Bensby et al. (2003) for the discrimination of stars according to their Galactic component to the cylindrical coordinate system (v_R, v_ϕ, v_z). For nearby stars, this adaptation is straightforward since the (v_R, v_ϕ, v_z) points to the same directions of the (U, V, W) vector in the solar neighborhood.

As Bensby et al. (2003), we use a velocity ellipsoid for the distribution of the joint velocity probability distribution function for each Galactic component:

$$f(v_R, v_\phi, v_z) = k \exp\left(-\frac{v_R^2}{2\sigma_{v_R}^2} - \frac{(v_\phi - v_c - V_{\text{asym}})^2}{2\sigma_{v_\phi}^2} - \frac{v_z^2}{2\sigma_{v_z}^2}\right), \quad (\text{B1})$$

where $k = ([2\pi]^{3/2} \sigma_{v_R} \sigma_{v_\phi} \sigma_{v_z})^{-1}$ is a normalization constant and v_c is the local circular velocity. The values to be used in Equation (B1) for each Galactic component are given in Table 1, taken from Kordopatis et al. (2013) and Amarante et al. (2020b). This equation allows us to calculate the thick-disk-to-thin-disk (TD/D) and the thick-disk-to-halo (TD/H) membership ratios for each star using Equation (3) from Bensby et al. (2003). We use these membership ratios to select thick-disk and halo candidate stars from our sample of planet-host stars.

Appendix C Catalog of Thick-disk and Halo Candidates

Table 2 provides a list of planet-host stars classified as thick-disk or halo stars. The columns Gaia EDR3 ID, RA, DEC, and Distance (see Appendix A) are obtained from GEDR3. The columns RV, [Fe/H], T_{eff} and $\log g$ are obtained from the surveys indicated by the symbol over the RV value. The Classification (Class.) indicates the Galactic component and the kinematic method used to classify it. The other columns are the derived orbital parameters, obtained as explained in Section 2.

Table 2
Table of Planet-host Stars Classified as Halo or Thick-disk Stars

Star Name	Gaia EDR3 ID	R.A.	Decl.	Distance	RV	[Fe/H]	T_{eff}	log g	Class.	E $\times 10^5$ ($\text{km}^2 \text{s}^{-2}$)	L_z $\times 10^3$ (kpc km s^{-1})	Ecc	(v_R, v_ϕ, v_z) (km s^{-1})	Z_{max} (kpc)	R_{apo} (kpc)	R_{peri} (kpc)
		(deg)	(deg)	(kpc)	(km s^{-1})		(K)	(cgs)								
BD+20 2457	625137162857354880	154.1867	19.8912	1.44	145.7 ^a				Halo	1.57	-0.23	0.91	(190.6, -26.4, -53.2)	6.38	0.59	12.78
HAT-P-12	1499514786891168640	209.3886	43.4933	0.141	-40.0 ^a				TD (a)	1.70	-1.30	0.34	(36.7, 158.0, 0.5)	0.15	4.16	8.41
HAT-P-12	1499514786891168640	209.3886	43.4933	0.141	-46.2 ^d	-0.26	4679	4.62	TD (a)	1.70	-1.28	0.34	(36.7, 155.7, -5.38)	0.18	4.07	8.4
HAT-P-26	3668036348641580288	213.1565	4.059	0.142	14.5 ^a				TD (a)	1.61	-1.56	0.30	(-86.7, 191.5, -26.3)	0.50	5.10	9.65
HAT-P-26	3668036348641580288	213.1565	4.059	0.142	10.9 ^d	0.03	5090	4.48	TD (a)	1.61	-1.56	0.30	(-85.1, 191.9, -29.1)	0.56	5.13	9.61
HD 111232	5855730584310531200	192.2160	-68.4247	0.029	104.5 ^a				TD (a)	1.67	-1.34	0.36	(-71.6, 163.1, -12.6)	0.19	4.19	8.94
HD 11755	558504529130235136	29.7078	73.1521	0.232	-87.6 ^a				TD (b)	1.49	-1.87	0.26	(-84.9, 224.0, -85.6)	2.72	6.71	11.49
HD 136418	1392396172224832896	229.7756	41.7323	0.104	-34.2 ^a				TD (a)	1.65	-1.45	0.32	(-72.8, 177.3, -4.0)	0.13	4.71	9.09
HD 233604	1023492257121204352	137.4535	53.5682	0.857	-73.7 ^a				TD (a)	1.51	-1.86	0.33	(-107.5, 209.9, 17.9)	1.04	5.97	11.87
HD 233604	1023492257121204352	137.4535	53.5682	0.857	-77.2 ^d	-0.29	4804	2.43	TD (a)	1.50	-1.85	0.33	(-110.3, 209.1, 15.21)	1.01	5.90	11.9
HD 47536	5583831735369515008	99.4489	32.3394	0.124	79.7 ^a				TD (a)	1.65	-1.42	0.28	(44.3, 171.1, 54.9)	1.24	4.87	8.64
HD 5583	363012289421389056	14.4870	34.9853	0.216	11.9 ^a				TD (a)	1.63	-1.42	0.36	(89.2, 170.1, -36.8)	0.76	4.44	9.61
HD 5891	2788816827588309120	15.1383	20.2923	0.278	-96.2 ^a				TD (a)	1.66	-1.34	0.35	(-64.7, 161.1, 33.2)	0.67	4.26	8.98
K2-111	53006669599267328	59.8903	21.2985	0.198	-16.7 ^a				TD (b)	1.69	-1.24	0.34	(13.9, 147.9, 67.4)	1.77	4.18	8.43
K2-15	3896271842760486272	178.1106	4.2547	0.498	-9.9 ^d	-0.25	5053	4.68	TD (a)	1.65	-1.37	0.31	(62.1, 167.0, -48.3)	1.38	4.61	8.84
K2-166	3701015375282968064	185.1880	2.2823	0.479	-8.7 ^d	-0.19	5915	3.93	TD (a)	1.64	-1.44	0.29	(62.6, 177.2, -27.9)	0.82	4.85	8.85
K2-204	2533185974768028032	17.3825	-0.5177	0.547	-50.6 ^c	-0.10	5746	4.16	TD (a)	1.63	-1.51	0.30	(-69.2, 180.6, 16.0)	0.58	5.00	9.30
K2-271	655863775507590400	125.2239	16.0908	0.538	-75.9 ^d	-0.48	5496	4.17	TD (a)	1.54	-1.68	0.36	(-112.6, 194.7, -35.8)	0.91	5.24	11.3
K2-86	55994798604873216	51.5531	18.6356	0.254	122.5 ^a				TD (a)	1.51	-1.78	0.39	(130.9, 211.4, -17.4)	0.37	5.38	12.40
K2-86	55994798604873216	51.5531	18.6356	0.254	122.4 ^c	-0.43	5030	4.47	TD (a)	1.50	-1.78	0.39	(130.7, 211.4, -17.4)	0.37	5.38	12.40
K2-86	55994798604873216	51.5531	18.6356	0.254	115.2 ^d	-0.30	5211	4.48	TD (a)	1.51	-1.77	0.37	(123.7, 209.8, -13.0)	0.27	5.41	11.9
KIC 5437945	2102070660978313472	288.4750	40.6513	1.298	-88.4 ^d	-0.75	7662	4.14	TD (a)	1.65	-1.37	0.19	(-10.4, 174.0, -89.9)	2.30	5.41	8.08
Kepler-10	2132155017099178624	285.6793	50.2415	0.186	-98.1 ^a				TD (a)	1.71	-1.26	0.36	(37.2, 153.7, 1.9)	0.08	3.98	8.38

Table 2
(Continued)

Star Name	Gaia EDR3 ID	R.A.	Decl.	Distance	RV	[Fe/H]	T_{eff}	log g	Class.	E $\times 10^5$ ($\text{km}^2 \text{s}^{-2}$)	L_z $\times 10^3$ (kpc km s^{-1})	Ecc	(v_R, v_ϕ, v_z) (km s^{-1})	Z_{max} (kpc)	R_{apo} (kpc)	R_{peri} (kpc)
		(deg)	(deg)	(kpc)	(km s^{-1})		(K)	(cgs)								
Kepler-10	2132155017099178624	285.6793	50.2415	0.186	-98.6 ^b	-0.13	5685	4.50	TD (a)	1.71	-1.26	0.36	(37.3, 153.2, 1.7)	0.08	3.96	8.38
Kepler-10	2132155017099178624	285.6793	50.2415	0.186	-104.1 ^d	-0.25	5623	4.18	TD (a)	1.71	-1.21	0.37	(38.0, 148.2, 0.0)	0.08	3.77	8.37
Kepler-112	2078722600285671936	296.9811	43.2097	0.511	-92.3 ^d	-0.62	5484	4.11	TD (b)	1.66	-1.38	0.23	(16.7, 170.0, -69.2)	1.68	5.01	8.17
Kepler-1228	2080534148769345408	296.5528	46.9662	0.513	-89.2 ^d	-0.39	5011	4.64	TD (b)	1.68	-1.12	0.44	(-79.7, 138.2, 66.2)	1.82	3.49	8.97
Kepler-1258	2132156632006693504	285.4049	49.9948	0.707	-66.8 ^d	-0.49	5736	4.25	TD (a)	1.62	-1.52	0.32	(88.1, 186.8, 6.2)	0.29	4.89	9.56
Kepler-1390	2086485186737501696	298.6624	48.2488	0.735	-62.7 ^d	-0.17	5392	4.21	TD (a)	1.61	-1.56	0.31	(89.8, 191.4, -3.89)	0.19	5.04	9.71
Kepler-1466	2126944603296783232	289.8312	44.6098	0.629	-99.8 ^d	-0.51	5660	4.39	TD (a)	1.69	-1.30	0.30	(21.9, 160.8, -40.8)	0.82	4.35	8.17
Kepler-1519	2086851495906130176	296.6679	49.4617	1.492	-83.2 ^b	-0.37	5467	3.90	TD (b)	1.62	-1.50	0.25	(-56.8, 183.9, -68.6)	1.77	5.35	8.97
Kepler-1559	2125705488052032640	292.2867	42.0726	0.622	-85.5 ^b	0.07	5223	4.53	TD (b)	1.58	-1.49	0.42	(130.2, 184.6, 13.4)	0.28	4.41	10.92
Kepler-1619	2105921803532722432	285.7036	44.4222	0.736	-16.7 ^b	-0.34	5634	4.18	TD (b)	1.36	-2.13	0.48	(158.9, 264.1, -7.0)	0.53	5.97	17.19
Kepler-1619	2105921803532722432	285.7036	44.4222	0.735	-25.0 ^d	-0.29	5738	4.14	TD (b)	1.38	-2.06	0.47	(160.3, 256.0, -9.49)	0.55	5.81	16.51
Kepler-1638	2134726877877965568	295.4823	48.5245	1.508	-93.7 ^b	-0.50	5534	4.12	TD (b)	1.70	-1.18	0.39	(51.6, 144.9, 38.3)	0.86	3.66	8.50
Kepler-177	2106339927188171776	286.0471	45.0532	1.451	-114.5 ^b	-0.23	5626	3.98	TD (b)	1.71	-1.18	0.36	(44.2, 148.0, -53.5)	1.41	3.86	8.25
Kepler-213	2127001056345369984	290.8242	44.6473	0.620	-82.5 ^d	0.11	5570	4.18	TD (a)	1.64	-1.41	0.34	(83.1, 174.9, 14.4)	0.28	4.49	9.21
Kepler-29	2086435189017387264	298.3483	47.4913	0.873	-59.4 ^d	-0.63	5296	4.21	TD (a)	1.60	-1.57	0.31	(90.2, 193.1, 6.3)	0.21	5.09	9.73
Kepler-329	2079224424266279936	299.2682	45.2273	0.439	-102.8 ^d	-0.46	4755	4.46	TD (b)	1.67	-1.28	0.28	(-22.2, 157.7, -87.6)	2.28	4.71	8.38
Kepler-390	2101638759069485568	291.6288	41.2088	0.429	-48.8 ^b	-0.11	5240	4.64	TD (a)	1.52	-1.79	0.34	(112.4, 220.9, 31.5)	0.68	5.70	11.51
Kepler-390	2101638759069485568	291.6288	41.2088	0.429	-60.0 ^d	-0.09	5178	4.53	TD (a)	1.54	-1.70	0.35	(114.9, 210.4, 29.3)	0.61	5.36	11.1
Kepler-392	2102948483573807616	288.6608	43.3682	0.685	-73.7 ^d	-0.70	5873	4.09	TD (a)	1.57	-1.61	0.35	(111.8, 200.0, -14.5)	0.39	5.06	10.5
Kepler-461	2126801563705846528	292.2491	46.1648	0.691	-111.0 ^b	-0.11	5769	4.38	TD (b)	1.72	-1.19	0.36	(-2.7, 146.3, -45.2)	0.94	3.82	8.13
Kepler-461	2126801563705846528	292.2491	46.1648	0.691	-117.1 ^d	-0.30	5681	4.07	TD (b)	1.72	-1.13	0.38	(-1.9, 139.9, -46.6)	0.98	3.60	8.13
Kepler-611	2106443453079518336	286.0049	45.4803	1.373	-36.8 ^b	0.12	5554	3.99	TD (a)	1.57	-1.64	0.33	(-105.6, 205.1, -14.3)	0.56	5.25	10.47
Kepler-646	2126970579257130112	290.4715	44.3870	0.459	-98.2 ^d	-0.47	5439	4.40	TD (b)	1.67	-1.37	0.26	(29.0, 169.0, -59.8)	1.37	4.83	8.28

Table 2
(Continued)

Star Name	Gaia EDR3 ID	R.A.	Decl.	Distance	RV	[Fe/H]	T_{eff}	log g	Class.	E $\times 10^5$ ($\text{km}^2 \text{s}^{-2}$)	L_z $\times 10^3$ (kpc km s^{-1})	Ecc	(v_R, v_ϕ, v_z) (km s^{-1})	Z_{max} (kpc)	R_{apo} (kpc)	R_{peri} (kpc)
		(deg)	(deg)	(kpc)	(km s^{-1})		(K)	(cgs)								
Kepler-660	2130882023153533184	288.1383	47.7246	0.564	-95.9^{b}	-0.27	4684	4.61	TD (a)	1.68	-1.32	0.36	(72.2, 162.6, -6.7)	0.23	4.14	8.87
Kepler-749	2076090506891080704	299.8973	43.9041	0.750	-53.2^{d}	-0.65	4868	4.29	TD (b)	1.50	-1.68	0.44	(147.9, 207.8, 25.9)	0.55	4.90	12.69
Kepler-966	2087263361789975040	297.2705	50.1218	1.042	-88.8^{b}	-0.10	5646	4.21	TD (a)	1.70	-1.29	0.33	(28.2, 157.6, 12.3)	0.31	4.16	8.29
NGTS-4	2891248292906892032	89.5988	-30.8118	0.277	110.4^{a}				TD (a)	1.65	-1.45	0.25	(32.9, 173.6, -59.9)	1.42	5.14	8.59
NGTS-4	2891248292906892032	89.5988	-30.8118	0.277	111.6^{c}	-0.17	5135	4.49	TD (a)	1.65	-1.45	0.25	(33.4, 173.1, -60.3)	1.43	5.11	8.60
WASP-4	6535499658122055552	353.5629	-42.0618	0.272	58.8^{a}				TD (b)	1.72	-1.10	0.44	(-58.7, 135.5, -25.9)	0.53	3.27	8.23
XO-2 N	934346809278715776	117.0268	50.2251	0.150	47.7^{a}				TD (a)	1.67	-1.32	0.37	(69.0, 158.7, -1.2)	0.10	4.11	9.02
XO-2 N	934346809278715776	117.0268	50.2251	0.150	47.1^{b}	0.36	5160	4.27	TD (a)	1.67	-1.32	0.37	(68.5, 158.6, -1.43)	0.10	4.11	9.01
XO-2 S	934346740559239296	117.0310	50.2169	0.150	46.8^{a}				TD (a)	1.67	-1.32	0.37	(68.0, 158.7, -1.3)	0.10	4.11	9.02

Notes. The symbols.

^a (Gaia).

^b (APOGEE).








^c (GALAH).

^d (LAMOST) indicates the catalog from where the RV, [Fe/H], T_{eff} , and log g were obtained.

^e Classified as thick-disk star according to our kinematical criterion.

^f Classified as thick-disk star according to both kinematical criteria: our and the Bensby et al. (2003) adapted formalism (Appendix B). Stars with $TD/D > 10$ are classified as thick disk.

ORCID iDs

Hélio D. Perottoni  <https://orcid.org/0000-0002-0537-4146>
 João A. S. Amarante  <https://orcid.org/0000-0002-7662-5475>
 Guilherme Limberg  <https://orcid.org/0000-0002-9269-8287>
 Helio J. Rocha-Pinto  <https://orcid.org/0000-0002-5274-4955>
 Silvia Rossi  <https://orcid.org/0000-0001-7479-5756>
 Friedrich Anders  <https://orcid.org/0000-0003-4524-9363>
 Lais Borbolato  <https://orcid.org/0000-0003-3382-1051>

References

- Adibekyan, V. 2019, *Geosc*, **9**, 105
 Ahumada, R., Prieto, C. A., Almeida, A., et al. 2020, *ApJS*, **249**, 3
 Akeson, R. L., Chen, X., Ciardi, D., et al. 2013, *PASP*, **125**, 989
 Amarante, J. A. S., Beraldo e Silva, L., Debattista, V. P., & Smith, M. C. 2020a, *ApJL*, **891**, L30
 Amarante, J. A. S., Smith, M. C., & Boeche, C. 2020b, *MNRAS*, **492**, 3816
 Belokurov, V., Erkal, D., Evans, N. W., Koposov, S. E., & Deason, A. J. 2018, *MNRAS*, **478**, 611
 Belokurov, V., Sanders, J. L., Fattahi, A., et al. 2020, *MNRAS*, **494**, 3880
 Bensby, T., Feltzing, S., & Lundström, I. 2003, *A&A*, **410**, 527
 Beraldo e Silva, L., Debattista, V. P., Khachatryan, T., & Nidever, D. 2020, *MNRAS*, **492**, 4716
 Bhatiani, S., Dai, X., & Guerras, E. 2019, *ApJ*, **885**, 77
 Bignone, L. A., Helmi, A., & Tissera, P. B. 2019, *ApJL*, **883**, L5
 Binney, J., & Tremaine, S. 2008, *Galactic Dynamics* (2nd ed.; Princeton, NJ: Princeton University Press)
 Bland-Hawthorn, J., & Gerhard, O. 2016, *ARA&A*, **54**, 529
 Bonaca, A., Conroy, C., Cargile, P. A., et al. 2020, *ApJL*, **897**, L18
 Bonaca, A., Conroy, C., Wetzel, A., Hopkins, P. F., & Kereš, D. 2017, *ApJ*, **845**, 101
 Borucki, W. J., Koch, D., Basri, G., et al. 2010, *Sci*, **327**, 977
 Bovy, J. 2020, arXiv:2012.02169
 Bovy, J., Rix, H.-W., Liu, C., et al. 2012, *ApJ*, **753**, 148
 Brassier, R., & Mojszsis, S. J. 2020, *NatAs*, **4**, 492
 Buder, S., Sharma, S., Kos, J., et al. 2021, *MNRAS*, in press
 Carrillo, A., Hawkins, K., Bowler, B. P., Cochran, W., & Vanderburg, A. 2020, *MNRAS*, **491**, 4365
 Chacón, J., & Duong, T. 2018, *Multivariate Kernel Smoothing and Its Applications* (2nd edn.; Boca Raton, FL: CRC Press)
 Chen, D.-C., Xie, J.-W., Zhou, J.-L., et al. 2021, *ApJ*, **909**, 115
 Clarke, A. J., Debattista, V. P., Nidever, D. L., et al. 2019, *MNRAS*, **484**, 3476
 Cui, X.-Q., Zhao, Y.-H., Chu, Y.-Q., et al. 2012, *RAA*, **12**, 1197
 Dai, X., & Guerras, E. 2018, *ApJL*, **853**, L27
 Das, P., Hawkins, K., & Jofré, P. 2020, *MNRAS*, **493**, 5195
 Di Matteo, P., Haywood, M., Lehnert, M. D., et al. 2019, *A&A*, **632**, A4
 Di Stefano, R., Berndtsson, J., Urquhart, R., et al. 2020, arXiv:2009.08987
 Dotter, A., Chaboyer, B., Jevremović, D., et al. 2008, *ApJS*, **178**, 89
 Dressing, C. D., & Charbonneau, D. 2013, *ApJ*, **767**, 95
 Dressing, C. D., & Charbonneau, D. 2015, *ApJ*, **807**, 45
 Feuillet, D. K., Feltzing, S., Sahlholdt, C. L., & Casagrande, L. 2020, *MNRAS*, **497**, 109
 Fischer, D. A., & Valenti, J. 2005, *ApJ*, **622**, 1102
 Fiteni, K., Caruana, J., Amarante, J. A. S., Debattista, V. P., & Beraldo e Silva, L. 2021, *MNRAS*, **503**, 1418
 Gaia Collaboration, Brown, A. G. A., Vallenari, A., et al. 2021, *A&A*, **649**, A1
 Gallart, C., Bernard, E. J., Brook, C. B., et al. 2019, *NatAs*, **3**, 932
 Gan, T., Shporer, A., Livingston, J. H., et al. 2020, *AJ*, **159**, 160
 Gonzalez, G. 1997, *MNRAS*, **285**, 403
 Grand, R. J. J., Kawata, D., Belokurov, V., et al. 2020, *MNRAS*, **497**, 1603
 Haywood, M., Di Matteo, P., Lehnert, M. D., et al. 2018, *ApJ*, **863**, 113
 Helmi, A. 2020, *ARA&A*, **58**, 205
 Helmi, A., Babusiaux, C., Koppelman, H. H., et al. 2018, *Natur*, **563**, 85
 Homer, J., Wittenmyer, R. A., Hinse, T. C., & Marshall, J. P. 2014, *MNRAS*, **439**, 1176
 Hsu, D. C., Ford, E. B., Ragozzine, D., & Ashby, K. 2019, *AJ*, **158**, 109
 Ingrassia, G., Novati, S. C., de Paolis, F., et al. 2009, *MNRAS*, **399**, 219
 Kordopatis, G., Gilmore, G., Wyse, R. F. G., et al. 2013, *MNRAS*, **436**, 3231
 Li, C., Zhao, G., Zhai, M., & Jia, Y. 2018, *ApJ*, **860**, 53
 Limberg, G., Rossi, S., Beers, T. C., et al. 2021, *ApJ*, **907**, 10
 Lindegren, L., Bastian, U., Biermann, M., et al. 2021b, *A&A*, **649**, A4
 Lindegren, L., Klioner, S. A., Hernández, J., et al. 2021a, *A&A*, **649**, A2
 Lund, M. B., Pepper, J., & Stassun, K. G. 2015, *AJ*, **149**, 16
 Mackereth, J. T., Bovy, J., Leung, H. W., et al. 2019b, *MNRAS*, **489**, 176
 Mackereth, J. T., Schiavon, R. P., Pfeffer, J., et al. 2019a, *MNRAS*, **482**, 3426
 Maldonado, J., Villaver, E., & Eiroa, C. 2013, *A&A*, **554**, A84
 Matsuno, T., Aoki, W., & Suda, T. 2019, *ApJL*, **874**, L35
 Matsuno, T., Hirai, Y., Tarumi, Y., et al. 2021, arXiv:2101.07791
 McMillan, P. J. 2017, *MNRAS*, **465**, 76
 Montalbán, J., Mackereth, J. T., Miglio, A., et al. 2020, arXiv:2006.01783
 Mróz, P., & Poleski, R. 2018, *AJ*, **155**, 154
 Naidu, R. P., Conroy, C., Bonaca, A., et al. 2020, *ApJ*, **901**, 48
 Nayakshin, S. 2017, *PASA*, **34**, e002
 Niedzielski, A., Nowak, G., Adamów, M., & Wolszczan, A. 2009, *ApJ*, **707**, 768
 Petigura, E. A., Marcy, G. W., Winn, J. N., et al. 2018, *AJ*, **155**, 89
 Queiroz, A. B. A., Anders, F., Santiago, B. X., et al. 2018, *MNRAS*, **476**, 2556
 Raymond, S. N., Scalo, J., & Meadows, V. S. 2007, *ApJ*, **669**, 606
 Ricker, G. R., Winn, J. N., Vanderspek, R., et al. 2014, *Proc. SPIE*, **9143**, 914320
 Sharma, S., Bland-Hawthorn, J., Johnston, K. V., & Binney, J. 2011, *ApJ*, **730**, 3
 Skrutskie, M. F., Cutri, R. M., Stiening, R., et al. 2006, *AJ*, **131**, 1163
 Stassun, K. G., Collins, K. A., & Gaudi, B. S. 2017, *AJ*, **153**, 136
 Taylor, M. B. 2005, in *ASP Conf. Ser. 347, Astronomical Data Analysis Software and Systems XIV*, ed. P. Shopbell, M. Britton, & R. Ebert (San Francisco, CA: ASP), 29
 Teske, J. K., Thorngren, D., Fortney, J. J., Hinkel, N., & Brewer, J. M. 2019, *AJ*, **158**, 239
 Vasiliev, E. 2019, *MNRAS*, **482**, 1525
 Woolf, V. M., & Wallerstein, G. 2004, *MNRAS*, **350**, 575
 Wright, E. L., Eisenhardt, P. R. M., Mainzer, A. K., et al. 2010, *AJ*, **140**, 1868
 Xiang, M., Ting, Y.-S., Rix, H.-W., et al. 2019, *ApJS*, **245**, 34
 Zhu, W., & Dong, S. 2021, arXiv:2103.02127
 Zięliński, P., Niedzielski, A., Wolszczan, A., Adamów, M., & Nowak, G. 2012, *A&A*, **547**, A91